Jaesool Shim[1]*
Kisoo Yoo[1]*
Prashanta Dutta[2]

[1]School of Mechanical Engineering, Yeungnam University, Gyeongsan, Gyeonsanbukdo, South Korea
[2]School of Mechanical and Materials Engineering, Washington State University, Pullman, WA, USA

Received September 11, 2016
Revised November 3, 2016
Accepted November 4, 2016

Research Article

Steady-state protein focusing in carrier ampholyte-based isoelectric focusing: Part II—validation and case studies

In this study, we systematically investigate the validity and applicability of an analytical model developed for carrier ampholyte-based isoelectric focusing (IEF). Three different IEF cases are considered in order to evaluate the efficacy of the approximate analytical results by comparison with high-resolution computer simulations. In the first case, three proteins are separated in a narrow pH range (6–9) by using 50 carrier ampholytes. In the second and third cases, the separation of proteins is studied in broad pH range (3–10) IEF by using 100 carrier ampholytes. Results obtained from the approximate analytical models are in very good agreement with the numerical results for IEF separation of cardiac troponin I, albumin, and hemoglobin in both narrow and broad pH ranges. The sensitivity of the analytical model is also tested for different initial mass ratios of proteins to ampholytes. No appreciable differences are observed between the approximate analytical and numerical results within the mass ratio range studied. The effect of a nominal electric field and/or a nominal pH gradient on protein focusing is also examined to demonstrate the effectiveness of the analytical model. Our results indicate that the use of both nominal electric field and pH gradient will result in erroneous peak concentrations for proteins. Finally, we describe the limitations of the approximate analytical solutions.

Keywords:
Analytical results / Carrier ampholytes / Isoelectric focusing / Protein
DOI 10.1002/elps.201600420

1 Introduction

Isoelectric focusing (IEF) has been widely used in the separation and concentration of RNA, proteins, bacteria, viruses, etc. by using an external electric field in the presence of a pH gradient [1]. Although IEF has been carried out on different platforms [2, 3], microscale IEF [4, 5] has attracted significant interest because of the much smaller volume of the separation channel. For instance, the microchannel or capillary used for IEF separation requires much smaller samples and reagents, which reduces the cost significantly. Due to the smaller length scale, faster separation of proteins can be achieved with a much higher resolution [6]. Furthermore, microscale IEF prevents severe sample degradation due to Joule heating [7] since a relatively smaller electric field strength is used for separation.

Modeling can be an efficient tool to design microchips for the efficient separation and concentration of proteins. The mathematical model for IEF and other electrophoretic techniques is well known from the seminal work of Bier et al. [8]. Since then, a number of research groups have simulated IEF in one-dimensional (1-D) geometry. Shimao [9] introduced steady-state IEF for the separation of proteins by using carrier ampholytes wherein the theory of isotachophoresis was modified to deal with the steady-state IEF model. The computer simulation tool GENTRANS [10], based upon the dynamic simulator of Bier et al. [8], was introduced to carry out IEF simulation under various conditions. For example, Mao et al. [11] demonstrated IEF simulation by using 140 individual carrier ampholytes, thus producing high-resolution focusing results. Subsequently, more realistic IEF modeling and simulation were introduced by employing realistic input parameters for carrier ampholytes (ΔpK value and absolute mobility) to reveal the variation of electric field strength after the end of separation, which is commonly known as the stabilizing phase [12, 13]. They particularly demonstrated that protein separation and focusing depend on the developed pH range. Later, Gas et al. [14] presented a comprehensive simulation package (SIMUL5) that can carry out both ITP and IEF simulation with any number of mono and multivalent electrolytes and ampholytes.

Recently, multi-dimensional IEF modeling and simulation was presented by Shim et al. [15]. They reported that the separation resolution of proteins can be changed with

Correspondence: Professor Prashanta Dutta, Ph.D., FASME, Mechanical and Materials Engineering, Washington State University, Pullman, WA 99164-2920
E-mail: prashanta@wsu.edu
Fax: +1-(509) 335-4662

*Equally contributing authors.

Colour Online: see the article online to view Figs. 1–7 in colour.

the channel shape. For example, different focusing efficiencies and resolution were obtained in the narrow and wide sections of a contraction–expansion channel. This research group also demonstrated that the protein separation can be affected by the concentration ratio between protein and carrier ampholytes due to the pH gradient distortion [16]. Lately, a variety of parallel algorithms has been introduced to handle hundreds of ampholytes to avoid distortion in the pH profile for IEF. These parallel algorithms can handle many amphoteric components, but the computation time has not been reduced significantly [17]. The computational cost will even be higher for realistic IEF simulation with a large number of ampholytes.

In the first paper in our two-paper series [18], we present approximate analytical solutions for carrier ampholyte-based IEF at the steady state. In this paper, we present finite-volume-based numerical results to test the validity of the analytical models for the spatial distribution of conductivity, pH-field, and electric field as well as for the concentration of proteins and ampholytes at the steady state. We also identified potential pitfalls of the analytical model for carrier ampholyte-based IEF. Comparisons are also presented for predictions based on the nominal and analytically found electric field and pH gradient. Here, the nominal pH gradient and nominal electric field strength are defined as $\frac{\Delta \mathrm{pH}}{L}$ and $\frac{\Delta V}{L}$, respectively, where ΔpH and ΔV are the pH range and voltage difference between anodic and cathodic reservoir.

2 Materials and methods

2.1 Mathematical model for carrier ampholyte-based IEF

In the absence of a bulk fluid flow, ampholyte-based IEF can be described by a set of mass conservation equations and a charge conservation equation. At the steady state, the mass conservation equations for each amphoteric component (ampholytes or proteins) can be given as [12]

$$\nabla \cdot \left[-D_i \nabla C_i + (\langle \mu_i \rangle \nabla \varphi) C_i \right] = 0 \tag{1}$$

where C_i, D_i, and $\langle \mu_i \rangle$ are the concentration, diffusion coefficient, and effective electrophoretic mobility of amphoteric component i, respectively. The concentration of the ith component (C_i) can be obtained by summing all $J_i + 1$ species (S_{ij}) in the system with a total of J_i dissociable groups as follows:

$$C_i = \sum_{j=1}^{J_i+1} S_{ij}. \tag{2}$$

The effective mobility ($\langle \mu_i \rangle$) of an amphoteric component can be defined as

$$\langle \mu_i \rangle = \sum_{j=1}^{J_i+1} \mu_{ij} S_{ij} / C_i \tag{3}$$

where μ_{ij} is the electrophoretic mobility of the jth species that make up each ith component in the system. The electrophoretic mobility can be found from the absolute mobility (ω_{ij}) and valence (z_{ij}) as follows:

$$\mu_{ij} = z_{ij} \omega_{ij}. \tag{4}$$

The electric potential (ϕ) of the electromigration term in Eq. (1) can be obtained from the following charge conservation equation:

$$\nabla \cdot \left[\nabla (\sigma \varphi) + F \left(\sum_{i=1}^{N} D_i \langle z_i \rangle \nabla C_i \right) \right] = 0 \tag{5}$$

where N is the total number of components and F is the Faraday constant. The effective valence for both the ampholyte and protein can be given as

$$\langle z_i \rangle = \sum_{j=1}^{J_i+1} z_{ij} S_{ij} / C_i. \tag{6}$$

In Eq. (5), the ionic conductivity of the buffer solution is

$$\sigma = F \left[\sum_{i=1}^{N} \sum_{j=1}^{J_i+1} z_{ij} \mu_{ij} S_{ij} + \omega_{\mathrm{H}^+} C_{\mathrm{H}^+} + \omega_{\mathrm{OH}^-} C_{\mathrm{OH}^-} \right] \tag{7}$$

where the subscripts H^+ and OH^- denote hydrogen and hydroxyl ions dissolved into the buffer solution. The concentration of hydrogen ions can be found from the local pH as

$$C_{\mathrm{H}^+} = 10^{-\mathrm{pH}} \tag{8}$$

and the concentration of the hydroxyl ions can be derived from the hydrogen ions using the following equilibrium equations:

$$C_{\mathrm{H}^+} C_{\mathrm{OH}^-} = K_w \tag{9}$$

where K_w is the dissociation constant.

The aforementioned mathematical model is based on some key but reasonable assumptions. First, the model neglects the Joule heating effect because relatively small electric fields are used to carry out protein separation at microscale IEF. Second, electro-osmotic flow is negligible. This assumption is rational because most experimental separation channels are coated with methyl cellulose or other chemicals in order to suppress electroosmosis [5, 6]. Third, carrier ampholytes are selected based on two dissociation constants. Fourth, all proteins are considered to be point masses so that surface charge distribution (e.g., dipole, quadrupole, and octupole) is not taken into account. Fifth, the buffer electrolyte used for the IEF separation is very dilute. Thus, the Nernst–Planck equation used for amphoteric components is applicable.

2.2 Numerical model for IEF simulation

A finite-volume-based method was used in this study to solve coupled mass and charge conservation equations. Details of

the numerical scheme and validations are presented in our earlier publications for carrier ampholyte-based IEF [15, 16]. Briefly, discretized algebraic equations are obtained at each grid point using the power law scheme for the mass and charge conservation equations. The system of algebraic equations is solved by using a tridiagonal matrix algorithm to obtain the concentration of each component and the electric potential at each grid point. Since all governing equations are nonlinearly coupled, an iterative scheme is used until the converged results are obtained for each variable. In our simulation, the convergence criteria were set at 10^{-5} and 10^{-4} for the concentration and electric potential, respectively. Grid-independent results were obtained by successively doubling the number of volume elements until the changes are less than 0.1%.

2.3 Steady-state analytical solutions for amphoteric components

Since IEF is a nonlinear process, the determination of exact analytical expressions is not possible. In the first paper of our two-paper series [18], approximate analytical expressions are presented in order to find the concentration of proteins and ampholytes in the separation channel. In the following sections, we briefly review the necessary analytical expressions and the key approximations used to obtain the analytical results.

2.3.1 Assumptions and approximations

The following assumptions and approximations are made in order to derive approximate analytical expressions [18].

(i) The steady-state concentration profiles for proteins and ampholytes are assumed to be Gaussian.
(ii) For steady-state concentration of protein, the electric field and the pH gradient remain constant within the focused band region. However, we did not use the nominal values of the electric field and pH gradient in our approximate analytical results.
(iii) At the steady state, the concentration of ampholytes at a particular location does not change regardless of the existence of proteins in the separation channel.
(iv) The spatial (ionic) conductivity distribution due to ampholytes is known from the ampholyte information as input data.
(v) The spatial distribution of the hydronium ion concentration remains the same in the absence and presence of proteins.
(vi) The effective electric field and effective pH gradient are obtained by averaging the Gaussian-like electric field and pH gradient profiles.

2.3.2 Ampholyte concentration

Based on the Gaussian distribution, the steady-state concentration distribution for ampholytes can be expressed as [18]

$$C_a = \frac{L \cdot C_{a,t=0}}{\sqrt{2\pi}\,\sigma_a} e^{-\frac{1}{2}\left(\frac{x-x_{fa}}{\sigma_a}\right)^2} \tag{10}$$

where L is the length of the separation channel; x and x_{f_a} are the position along the separation channel and the focusing location of the ampholyte, respectively; and $C_{a,t=0}$ is the initial concentration of the ampholyte. The location of the inflection point for the focused ampholyte band is

$$\sigma_a = \sqrt{\left(\frac{D_a}{\omega_a}\right)\left(\frac{-1}{\left.\frac{\mathrm{d}\langle z_a\rangle}{\mathrm{dpH}}\right|_{x=\mathrm{p}I,a} \frac{\Delta\,\mathrm{pH}}{L}\left.E_x(x)\right|_{x=\mathrm{p}I,a}}\right)} \tag{11}$$

where $\frac{\Delta\,\mathrm{pH}}{L}$ is the nominal pH gradient and z_a is the effective valence of an ampholyte. The applied electric field can be found from

$$E_x(x)_a = \frac{I}{\kappa(x)_a} \tag{12}$$

where I is the applied current density and $\kappa(x)_a$ is the ionic conductivity distribution due to ampholytes only. For a biprotic ampholyte, the slope of the titration curve at the focusing point is

$$\left.\frac{\mathrm{d}z_a}{\mathrm{dpH}}\right|_{x=\mathrm{p}I,a} = -\frac{2ln(10)}{2+10^{\Delta\,\mathrm{p}K/2}} \tag{13}$$

2.3.3 Protein concentration

Like ampholyte, the concentration distribution of proteins can be given as [18]

$$C_p = \frac{L \cdot C_{p,\,t=0}}{\sqrt{2\pi}\sigma_p} e^{-\frac{1}{2}\left(\frac{x-x_{fp}}{\sigma_p}\right)^2} \tag{14}$$

where x_{fp} is the focusing point of the protein and $C_{p,t=0}$ is the initial concentration of the protein. The location of the inflection point for the focused protein band is given as

$$\sigma_p = \sqrt{\left(\frac{RT}{F}\right)\left(\frac{-1}{\left.\frac{\mathrm{d}\langle z_i\rangle}{\mathrm{dpH}}\right|_p \frac{\Delta\,\mathrm{pH}}{L}\left(\left.(E_x)_a\right|_{x=\mathrm{p}I,p}\right)\left(1-\chi\left(1-f_{e,p,\min}\right)\right)\left(1-\chi\left(1-f_{\mathrm{pH},p,\min}\right)\right)}\right)}. \tag{15}$$

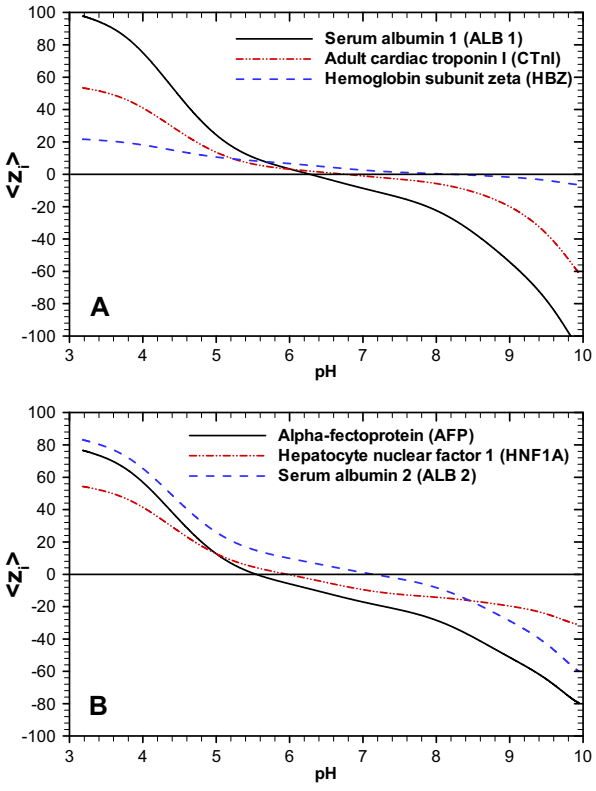

Figure 1. Titration curves for (A) serum albumin 1 (ALB 1, pI = 6.28), adult cardiac troponin I (cTnI, pI = 6.95), hemoglobin subunit zeta (HBZ, pI = 8.21), and (B) alpha-fetoprotein (AFP, pI = 5.542), hepatocyte nuclear factor 1 (HNF1A, pI = 5.965), and serum albumin 2 (ALB 2, pI = 7.138). Data for these protein titration curves were obtained from the protein data bank [19]. Methods for obtaining the mean square charge from the titration curve are explained in our previous work [16].

Here, R is the universal gas constant, T is the absolute temperature, $(E_x)_a|_{x=\mathrm{p}I,p}$ is the electric field at the pI point of the protein, and χ is a constant resulting from the averaging step of the Gaussian profiles. The correction factors for the electric field and pH gradient can be given as [18]

$$f_{e,p,\min} = \frac{\kappa_a}{\kappa_a + F\left(\langle z_p^2\rangle \omega_p C_p\right)_{\mathrm{pH}=\mathrm{p}I}} \tag{16}$$

$$f_{\mathrm{pH},p,\min} = \frac{\left(\sum \frac{\mathrm{d}\langle z_a\rangle}{\mathrm{d(pH)}}(C_a)\right)\Big|_{x=x_{fa}}}{\left(\sum \frac{\mathrm{d}\langle z_a\rangle}{\mathrm{d(pH)}}(C_a)\right)\Big|_{x=x_{fa}} + \sum \frac{\mathrm{d}\langle z_p\rangle}{\mathrm{d(pH)}^*} C_p(x)\Big|_{x=x_{fp}}} \tag{17}$$

Although the concentration of ampholytes can be computed explicitly from Eqs. (10) to (13), an iterative technique is required for the concentration distribution of proteins since Eqs. (14)–(17) are nonlinearly coupled. Details of finding ampholyte and protein concentration distributions are presented in [18], and will not be repeated.

3 Results and discussion

In this study, IEF simulations were carried out to evaluate the efficacy of the proposed approximate analytical solutions. Three different model systems were studied in a 2-cm-long separation channel. In the first model system, three plasma proteins, serum albumin 1 (ALB 1, pI = 6.28), adult cardiac troponin I (cTnI, pI = 6.95), and hemoglobin subunit zeta (HBZ, pI = 8.21), are separated in a narrow pH range (6)–(9) by using 50 biprotic carrier ampholytes. In the second system, the same three plasma proteins are separated in a broad pH range using 100 carrier ampholytes. Finally, in the third system, three other plasma proteins, alpha-fetoprotein (AFP, pI = 5.542), hepatocyte nuclear factor 1 (HNF1A, pI = 5.965), and serum albumin 2 (ALB 2, pI = 7.138), are separated in the broad pH range by using the same 100 carrier ampholytes. The titration curves for all proteins used in this study are shown in Fig. 1. The charge data were obtained from the protein data bank [19]. In both the numerical and analytical results, the initial concentration of each ampholyte was 0.45 [mM], while the initial concentration of each protein was 0.00225 [mM]. The absolute mobility of each protein was set at 2E–9 [m^2/Vs], while the absolute mobility of each ampholyte was assumed to be 3E–8 [m^2/Vs]. The diffusion coefficient of each amphoteric molecule is obtained from the absolute mobility by using the Nernst–Einstein equation [20].

3.1 Model system 1—Narrow pH range IEF

As previously mentioned, the pH range was created using 50 biprotic ampholytes with a $\Delta\,\mathrm{p}K = 3.0$. The electric potential difference between the anode and cathode was set as 300 V for which the steady-state current density was calculated as 58.78 [A/m^2]. Numerical and analytical results were obtained for three different initial concentration ratios of proteins-to-ampholytes (C_p/C_a): 1/200, 1/300, and 1/400. Figure 2 shows the spatial distribution of conductivity at the steady state considering all components in the system. The analytical conductivities are calculated by adding the protein conductivity information into the conductivity of pure ampholytes only. Thus, the local peaks at the location of the protein isoelectric point are due to the presence of proteins. As seen in Fig. 2, the analytically obtained conductivity values are almost identical to the numerical value, except at the location of the protein region. The peaks of proteins in analytical solution are slightly higher than that of the numerical peak because the analytical model does not consider the concentration reduction of ampholytes near protein focusing regions. It is well known that the focused concentration of ampholytes near protein regions is hindered due to the existence of proteins. However, the focused concentration of ampholytes away from the protein regions is not different regardless of the existence of proteins if the concentration of proteins is much smaller than that of the ampholytes [20]. Nevertheless, the analytical solutions are very close to the

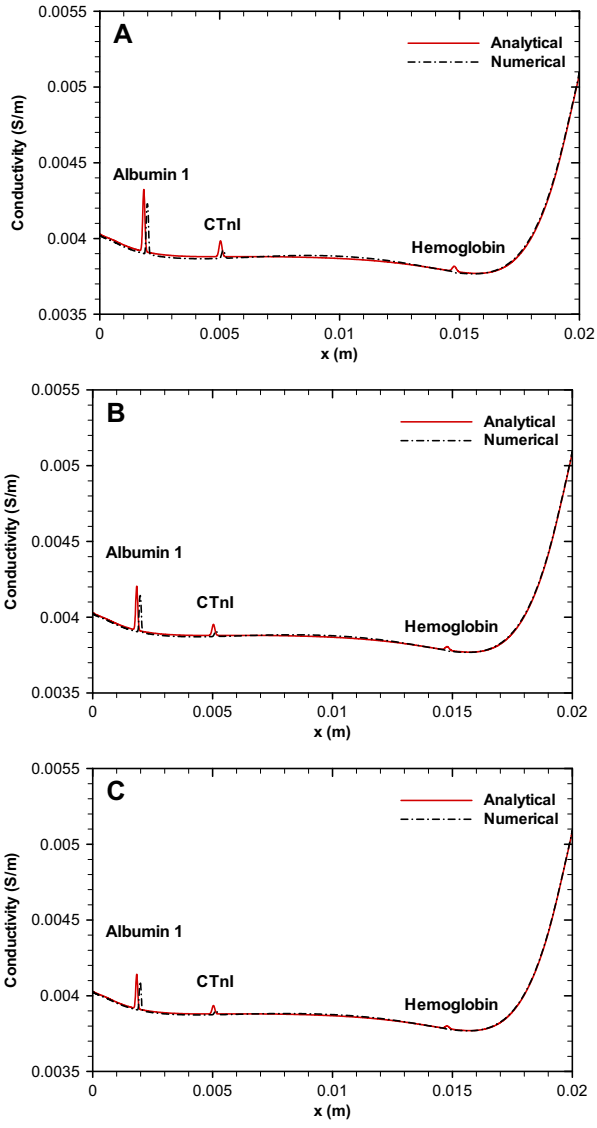

Figure 2. Comparison of conductivity profiles at the steady state for initial (A) C_p/C_a = 1/200, (B) C_p/C_a = 1/300, and (C) C_p/C_a = 1/400 in a narrow pH range (6–9) IEF. The analytically predicted conductivity distribution is slightly higher than the numerical one since in our analytical model we assumed that the concentration of ampholytes does not change in the presence of proteins.

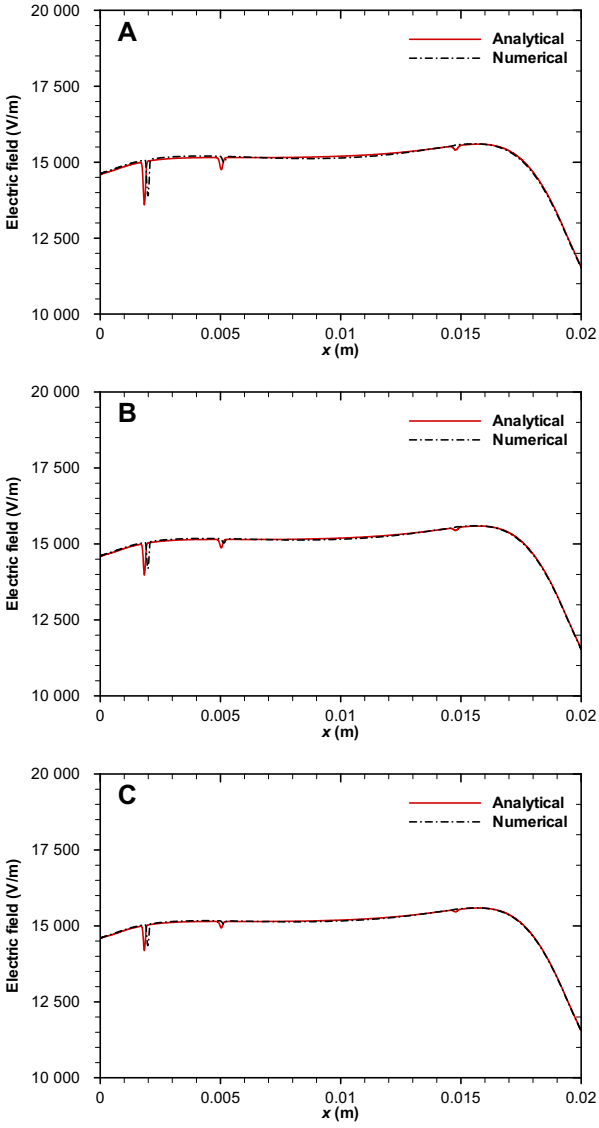

Figure 3. Comparison of electric field profiles at the steady state for initial (A) C_p/C_a = 1/200, (B) C_p/C_a = 1/300, and (C) C_p/C_a = 1/400 in a narrow pH range (6–9) IEF. The deviation between the analytical and numerical model is resulted from the conductivity distribution described earlier.

numerical results for all three different mass ratios of proteins to ampholytes.

Figure 3 shows the electric field profiles obtained from the analytical solution and the numerical simulation for the separation of three proteins in a narrow pH range. For the analytical solution, the electric fields were calculated from conductivity profiles shown in Fig. 2 using Eq. (12). The analytical solutions are very similar to the numerical simulations for all concentration ratios. We note that the nominal electric field for this case is 15 000 [V/m]. Thus, near the protein regions, the electric field values deviate from their nominal values by as much as 7% when the initial concentration of ampholytes is 200 times higher than that of the protein. As the initial concentration of protein decreases with respect to the initial concentration of ampholytes, the discrepancy between the nominal electric field and the actual electric field decreases in the protein region. However, at the right end of the separation channel, the nominal electric field is significantly different than the actual electric field due to the high ionic conductivity near pH 9. As shown in Eq. (7), the ionic conductivity is proportional to the concentration of ampholytes, hydrogen ions, and hydroxide ions. Although ampholytes form Gaussian bands with uniform peak heights throughout the separation channel, the concentration of hydroxyl ions increases with pH. For example, at pH 9, the concentration of hydroxide ions is 10^{-2} mM, which significantly contributes to ionic conductivity. Consequently, ionic

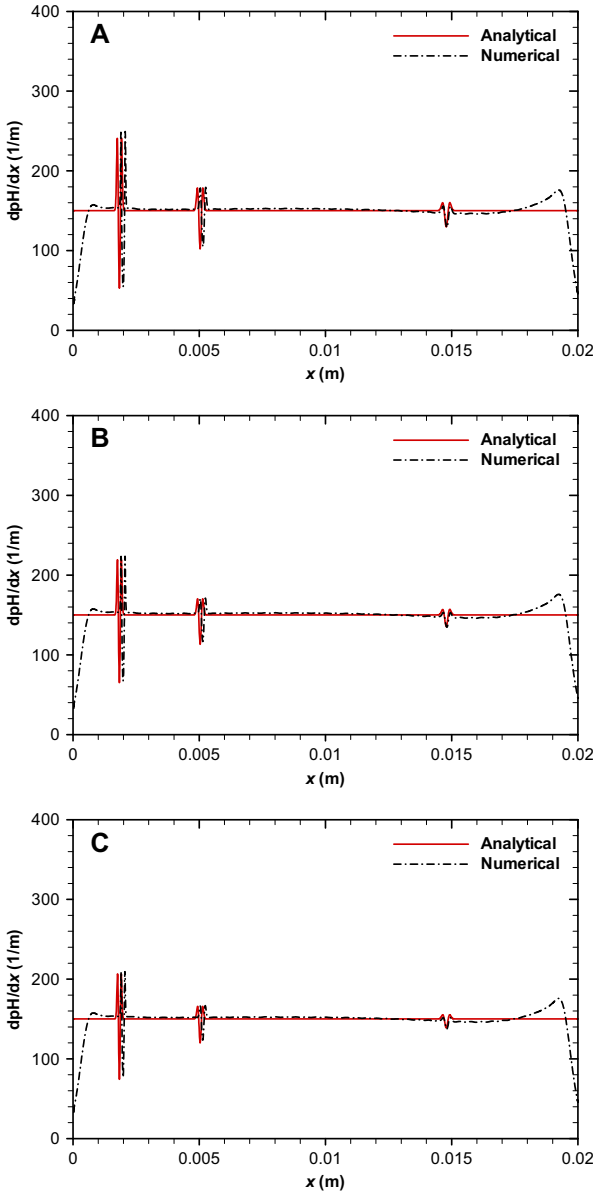

Figure 4. Comparison of pH gradient ($\frac{dpH}{dx}$) profiles at the steady state for initial (A) $C_p/C_a = 1/200$, (B) $C_p/C_a = 1/300$, and (C) $C_p/C_a = 1/400$ in a narrow pH range (6–9) IEF.

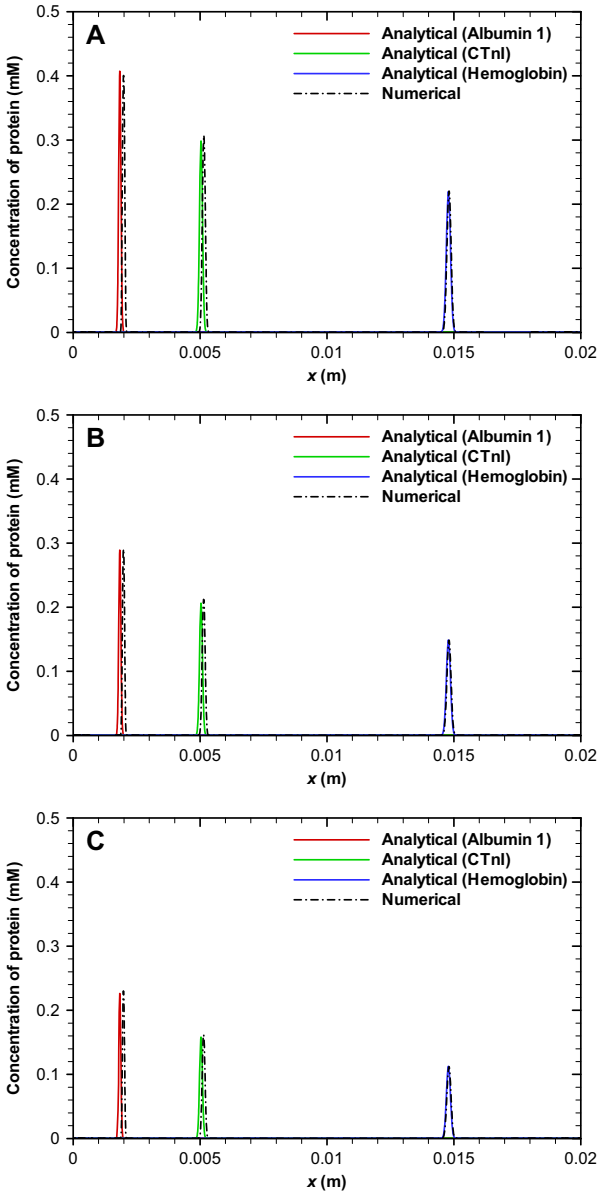

Figure 5. Comparison of protein concentration profiles at the steady state for initial (A) $C_p/C_a = 1/200$, (B) $C_p/C_a = 1/300$, and (C) $C_p/C_a = 1/400$ in a narrow pH range (6–9) IEF.

conductivity significantly increases near the right end (see Fig. 2), resulting in a large deviation in the electric field with respect to the nominal electric field. Our analytical model was able to capture the electric field accurately for all cases presented here, which is a major strength of the presented analytical model.

The pH gradient ($\frac{dpH}{dx}$) profiles obtained from analytical solutions and numerical simulations are shown in Fig. 4. Remarkably, both the numerical and analytical solutions capture the fluctuations in the pH gradients at the protein regions. The analytical solution deviates greatly from the numerically predicted value at both ends of the separation region. Thus, this analytical model should not be used to obtain protein concentration when the p*I* points of proteins are very close to the anode and cathode because the linear pH assumption along the channel is not satisfied in that region. Nevertheless, the analytical method is quite effective in capturing the variation in the pH gradient at the protein focusing regions, which are located away from the anode and cathode regions. Like the electric field, the nominal pH gradient value (150) deviates significantly from the actual pH gradients. For example, the pH gradient valley reaches 53.0, 65.4, and 76.5 at the p*I* locations of albumin as shown in Figs. 4(A), (B), and (C), respectively. Thus, the use of the nominal pH gradient value will result in a large error in the protein concentration profile.

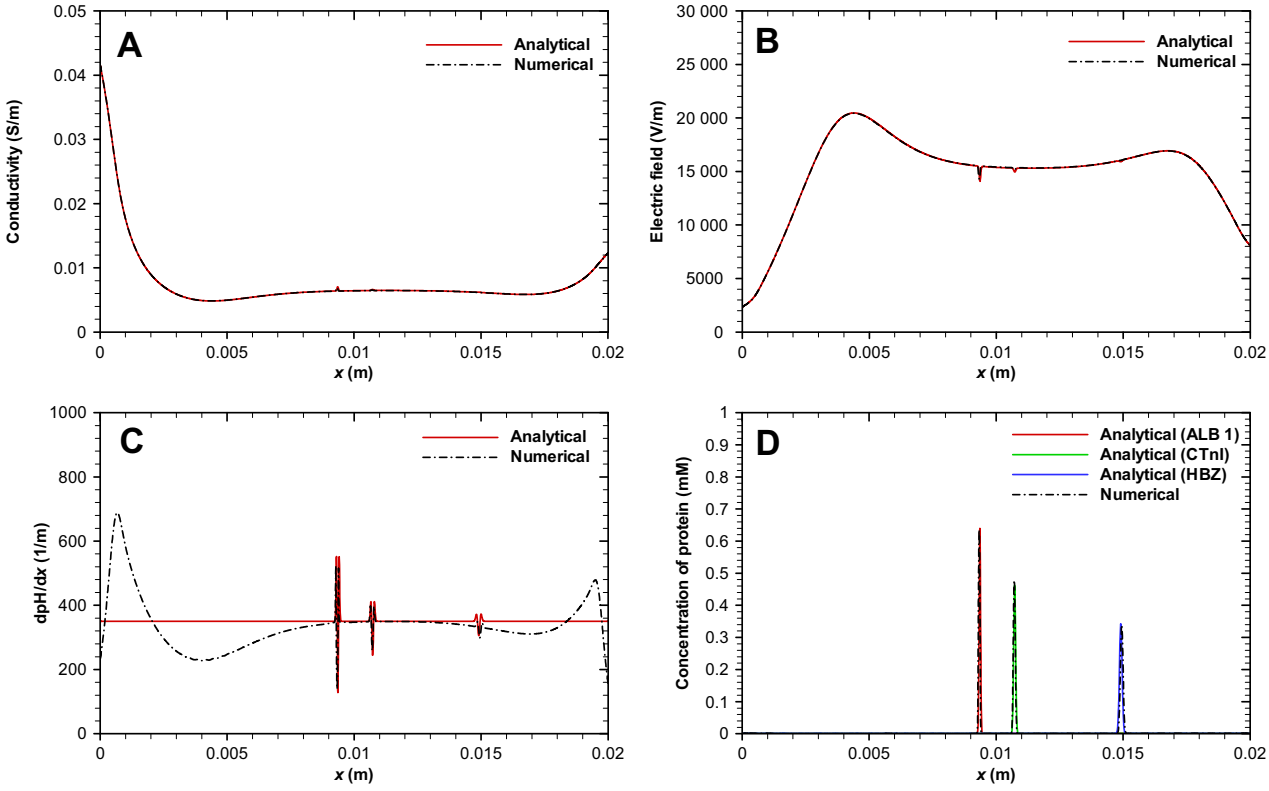

Figure 6. Comparison of analytical solution and numerical simulation at the steady state for initial $C_p/C_a = 1/200$ in a broad range (3–10) IEF for separation of serum albumin 1 (ALB 1, p$I = 6.28$), adult cardiac troponin I (cTnI, p$I = 6.95$), and hemoglobin subunit zeta (HBZ, p$I = 8.21$). (A) Local ionic conductivity, (B) local electric field, (C) local pH gradient, and (D) protein concentration profile.

Figure 5 shows the concentration profile of proteins at the steady-state condition. The analytical solution is in good agreement with the numerical simulation for all three cases presented here. For the peak heights, the highest percentage of errors between the analytical solution and numerical simulation are 1.75, 3.15, and 0.50% for albumin, cTnI, and hemoglobin, respectively. The discrepancy between the analytical and numerical solution increases slightly with the increase in the initial mass of proteins with respect to the initial mass of ampholyte. It is also interesting to note that the approximate analytical solutions are able to predict the focused band location within 2% of the numerical value. Considering the numerical uncertainty/error, our approximate analytical models are very effective in predicting the steady-state protein concentration distributions in this narrow pH range case.

3.2 Broad pH range (3–10) IEF

In this section, we present results for carrier ampholyte-based IEF in a broad pH range (3–10). One hundred biprotic ampholytes (ΔpK $= 3.0$) were used to create a pH profile in a 2 cm-long channel. Like model system 1, a potential difference of 300 V was applied between the anode and cathode reservoirs. For model system 2, the pI values of proteins are located between 6.28 and 8.21, while for model system 3, these values are bounded between 5.54 and 7.2. As in model system 1, three different cases were studied for both model 2 and model 3 based on the ratio of the initial mass of the protein to the initial mass of ampholytes (C_p/C_a): 1/200, 1/300, and 1/400. In both systems, the highest discrepancies between analytical solutions and numerical results are obtained for the initial $C_p/C_a = 1/200$. Thus, for the rest of the study, we only concentrate on the $C_p/C_a = 1/200$ case.

Figure 6 shows analytical solutions for the conductivity, electric field, pH gradient, and concentration of focused proteins for model system 2. For comparison, numerical results obtained from the finite-volume-based technique are also presented. The analytical solutions are in very good agreement with the numerical results for the ionic conductivity, electric field, and protein concentration distributions. However, the approximate analytical model failed to capture the correct distribution for the pH gradient close to the anolyte and catholyte reservoirs, though pH profiles are nearly indistinguishable (not shown). This is a major deviation from the narrow pH range results presented in an earlier section, in which the analytical model was able to capture the pH gradient much better. Thus, one has to be particularly careful in using this model for broad pH range IEF.

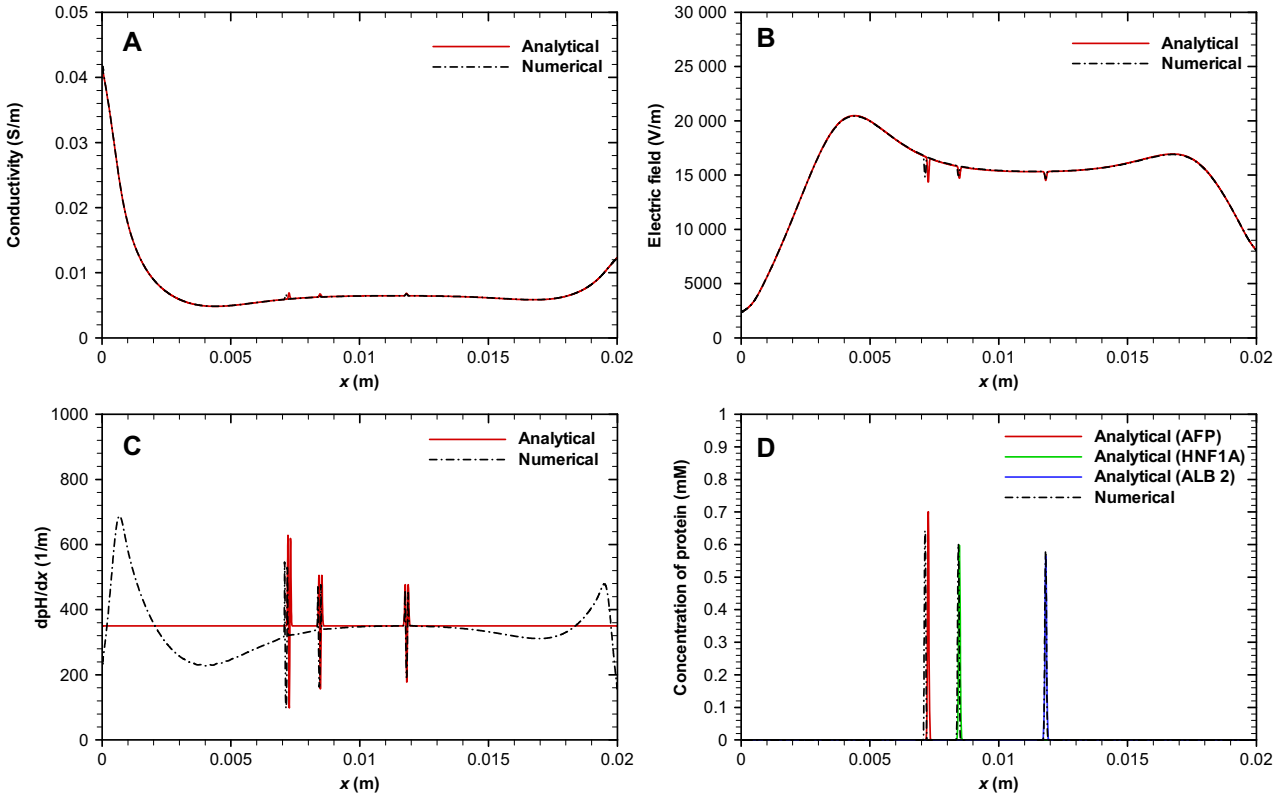

Figure 7. Comparison of analytical solution and numerical simulation at the steady state for initial $C_p/C_a = 1/200$ in a broad range (3–10) IEF for separation of alpha-fetoprotein (AFP, p$I = 5.542$), hepatocyte nuclear factor 1 (HNF1A, p$I = 5.965$), and serum albumin 2 (ALB 2, p$I = 7.138$). (A) Local ionic conductivity, (B) local electric field, (C) local pH gradient, and (D) protein concentration profile.

Very close to the anolyte and catholyte reservoirs, the pH gradient also deviated significantly in the narrow pH range (see Fig. 4). This deviation in pH gradient is due to the stringent assumptions used for the analytical solution. For example, we assumed that the pH profile is linear, and the local pH gradient can be calculated from the nominal pH gradient value with some local corrections. However, the pH gradient value deviates significantly from the nominal value where ampholytes are focused non-uniformly [16]. In reality, in broad range IEF, ampholytes are not focused in a Gaussian profile resulting in a concentration valley. The concept of a concentration valley was reported by Mosher and Thormann [12]. The non-uniform focusing of ampholytes at the concentration valley is responsible for a significant deviation in the pH gradient between the analytical and numerical predictions. Nevertheless, the deviations in the pH gradient between the analytical and numerical predictions are quite small at the location of protein p*I*s for model system 2 since the proteins were focused at the region of uniform ampholyte distribution. Moreover, the analytical model can capture the fluctuations in the pH gradient remarkably well at the location of the protein isoelectric points. Also, the protein concentration distribution matched very well between the analytical model and numerical simulation, as shown in Fig. 6(D). For protein peak heights, the deviation between the analytical and numerical work is 0.5, 3.25, and 0.23% for albumin, cTnI, and hemoglobin, respectively. Like model system 1, the electric field value deviates significantly from its nominal value due to the nonlinear interactions in IEF. For broad range IEF, the region of mismatch between the nominal electric field and actual electric field grows significantly, and the use of nominal electric field cannot be justified.

Results for model system 3 are shown in Fig. 7, where alpha-fetoprotein, hepatocyte nuclear factor 1, and serum albumin 2 are separated in a broad pH range of 3–10. In this case, the p*I* point of at least one protein (alpha-fetoprotein) is located in the region where the analytical results are not able to capture the pH gradient effectively. This particular case has been selected intentionally to reveal the limitation of the analytical model. The analytical solution over-predicted the pH gradient of alpha-fetoprotein, which is responsible for the large deviation in the analytical and numerical results for the concentration distribution of alpha-fetoprotein. The analytical results are in good agreement with the numerical results for the other two proteins (hepatocyte nuclear factor 1 and serum albumin 2) for which the predicted value for the pH gradient is very close between the numerical and analytical models. In other words, our approximate analytical method will be able to provide accurate results between $x = 0.8$ and 1.4 cm. Thus, it is very important to capture the appropriate pH gradient at the protein isoelectric point.

Table 1. Percentage errors between analytical solution and numerical simulation

pH: 6–9, $C_p/C_a = 1/200$	Percentage in error between analytical and numerical		
	Albumin (p*I* = 6.28)	CTnI (p*I* = 6.95)	Hemoglobin (p*I* = 8.21)
Analytical pH gradient and analytical electric field	1.496	3.149	0.227
Nominal pH gradient and analytical electric field	38.400	10.569	4.995
Analytical pH gradient and nominal electric field	6.468	1.302	3.546
Nominal pH gradient and nominal electric field	44.833	11.328	3.542

pH: 3–10, $C_p/C_a = 1/200$	Albumin (p*I* = 6.28)	CTnI (p*I* = 6.95)	Hemoglobin (p*I* = 8.21)
Analytical pH gradient and analytical electric field	0.471	3.243	0.234
Nominal pH gradient and analytical electric field	22.973	9.314	4.574
Analytical pH gradient and nominal electric field	6.599	0.837	1.001
Nominal pH gradient and nominal electric field	39.167	9.299	2.501

pH: 3–10, $C_p/C_a = 1/200$	Alpha-fetoprotein (p*I* = 5.542)	Hepatocyte nuclear factor 1-alpha (p*I* = 5.965)	Serum albumin 2 (p*I* = 7.138)
Analytical pH gradient and analytical electric field	9.375	0.664	2.586
Nominal pH gradient and analytical electric field	54.553	27.334	20.690
Analytical pH gradient and nominal electric field	14.648	3.536	1.724
Nominal pH gradient and nominal electric field	57.690	28.239	21.976

3.3 Nominal vs. actual for electric field and/or pH gradient in protein focusing

We also predicted the protein peak heights using the nominal electric field and/or nominal pH gradient, and compared them with the numerical results. Table 1 shows the percentage difference between the numerical predictions and results obtained from Eq. (14) based on various simplifications. For brevity, only the initial concentration ratio, $C_p/C_a = 1/200$ case is presented here. In a narrow pH range (6)–(9), the percentage error is highest (44.8%) for albumin when both the nominal pH gradient and nominal electric field values are used. A similar higher error (38.4%) is found for the albumin peak height if the nominal pH gradient is used along with the analytically predicted electric field. However, the error value decreases significantly if the nominal electric field is used along with the analytically calculated pH gradient. Of course, the use of both the analytically computed electric field and pH gradient provides the least error. The error trends are similar for the other two proteins, suggesting that the proper estimation of the pH gradient is the single most important factor for analytical calculations of the protein concentration at steady state. The same conclusions can be drawn for the broad pH system. As discussed previously, our analytical model overestimates the peak height for alpha fetoprotein due to incorrect estimation of the pH gradient at its isoelectric point.

4 Concluding remarks

Numerical results are presented in order to study the validity of the approximate analytical results for carrier ampholyte-based IEF. Both narrow and broad pH range cases were considered to demonstrate the applicability of the analytical model. The analytical model is very capable of predicting the steady-state protein concentration as well as the conductivity and electric field for a narrow pH range (6)–(9). The analytical model was also tested for different initial concentration ratios of protein to ampholytes. For all cases presented herein, the maximum error in the protein peak heights was less than 5% in a narrow pH range. The discrepancy between the numerical and analytical results grows with an increase in the initial mass ratio of protein to ampholyte. The approximate analytical model failed to predict the protein peak heights at the location close to the anode and cathode reservoirs where the pH profile is nonlinear due to the formation of a concentration valley. Nevertheless, the analytical model is much faster than the numerical model in predicting the IEF behavior in a microchannel for any number of ampholytes. The analytical model provides expressions for effective electric field and pH gradients, which are essential in order to obtain highly accurate protein peak heights analytically. Our study also shows that erroneous protein peak heights will result if a nominal pH gradient is used. The analytical model can also capture the nonlinear electric field distribution, which is significantly different than the nominal electric field.

This work was supported in part by a 2015 Yeungnam University Research Grant and in part by the US National Science Foundation under grant no. DMS 1317671.

The authors have declared no conflict of interest.

5 References

[1] Righetti, P. G., *Isoelectric Focusing : Theory, Methodology, and Applications*, Elsevier, Amsterdam 1983.

[2] Bjellqvist, B., Ek, K., Righetti, P. G., Gianazza, E., Görg, A., Westermeier, R., Postel, W., *J. Biochem. Biophys. Methods* 1982, *6*, 317–339.

[3] Righetti, P. G., *Immobilized pH Gradients: Theory and Methodology*, Elsevier, New York 1990.

[4] Herr, A. E., Molho, J. I., Drouvalakis, K. A., Mikkelsen, J. C., Utz, P. J., Santiago, J. G., Kenny, T. W., *Anal. Chem.* 2003, *75*, 1180–1187.

[5] Cui, H., Horiuchi, K., Dutta, P., Ivory, C. F., *Anal. Chem.* 2005, *77*, 1303–1309.

[6] Cui, H. C., Horiuchi, K., Dutta, P., Ivory, C. F., *Anal. Chem.* 2005, *77*, 7878–7886.

[7] Rathore, A. S., *J. Chromatogr. A* 2004, *1037*, 431–443.

[8] Bier, M., Palusinski, O., Mosher, R., Saville, D., *Science Science* 1983, *219*, 1281–1287.

[9] Shimao, K., *Electrophoresis* 1987, *8*, 14–19.

[10] Thormann, W., Caslavska, J., Mosher, R. A., *J. Chromatogr. A* 2007, *1155*, 154–163.

[11] Mao, Q. L., Pawliszyn, J., Thormann, W., *Anal. Chem.* 2000, *72*, 5493–5502.

[12] Mosher, R. A., Thormann, W., *Electrophoresis* 2002, *23*, 1803–1814.

[13] Mosher, R. A., Thormann, W., *Electrophoresis* 2008, *29*, 1036–1047.

[14] Hruska, V., Jaros, M., Gas, B., *Electrophoresis* 2006, *27*, 984–991.

[15] Shim, J., Dutta, P., Ivory, C. F., *Electrophoresis* 2007, *28*, 572–586.

[16] Yoo, K., Shim, J., Liu, J., Dutta, P., *Electrophoresis* 2014, *35*, 638–645.

[17] Shim, J., Dutta, P., Ivory, C. F., *J. Mech. Sci. Technol.* 2009, *23*, 3169–3178.

[18] Shim, J., Yoo, K., Dutta, P., *Electrophoresis* 2017. doi:10.1002/elps.201600416.

[19] http://www.uniprot.org.

[20] Mosher, R. A., Saville, D. A., Thormann, W., *The Dynamics of Electrophoresis*. VCH, Weinheim 1992.

